

Linear microbunching analysis for recirculation machines

C.-Y. Tsai,^{1,*} D. Douglas,² R. Li,^{1,2} and C. Tennant²

¹*Department of Physics, Virginia Tech, Blacksburg, Virginia 24061, USA*

²*Jefferson Laboratory, Newport News, Virginia 23606, USA*

(Received 21 March 2016; published 28 November 2016)

Microbunching instability (MBI) has been one of the most challenging issues in designs of magnetic chicanes for short-wavelength free-electron lasers or linear colliders, as well as those of transport lines for recirculating or energy-recovery-linac machines. To quantify MBI for a recirculating machine and for more systematic analyses, we have recently developed a linear Vlasov solver and incorporated relevant collective effects into the code, including the longitudinal space charge, coherent synchrotron radiation, and linac geometric impedances, with extension of the existing formulation to include beam acceleration. In our code, we semianalytically solve the linearized Vlasov equation for microbunching amplification factor for an arbitrary linear lattice. In this study we apply our code to beam line lattices of two comparative isochronous recirculation arcs and one arc lattice preceded by a linac section. The resultant microbunching gain functions and spectral responses are presented, with some results compared to particle tracking simulation by ELEGANT (M. Borland, APS Light Source Note No. LS-287, 2002). These results demonstrate clearly the impact of arc lattice design on the microbunching development. The underlying physics with inclusion of those collective effects is elucidated and the limitation of the existing formulation is also discussed.

DOI: [10.1103/PhysRevAccelBeams.19.114401](https://doi.org/10.1103/PhysRevAccelBeams.19.114401)

I. INTRODUCTION

The beam quality preservation is of general concern in delivering a high-brightness electron beam through a transport line or recirculation arc in the design of modern accelerators. In the high-brightness beam transport, the initial small density modulations can be converted into energy modulations due to short-ranged wakefields or high-frequency impedances. Then, the energy modulations would be transformed back to density counterparts downstream a dispersive region. The density-energy conversion, if forming a positive feedback, can result in the enhancement of modulation amplitudes. This has been known as the microbunching instability (MBI). MBI has been one of the most challenging issues associated with such beam line designs as magnetic bunch compressor chicanes for free-electron lasers or linear colliders. Moreover, it also poses difficulties in the design of transport lines for recirculation or energy-recovery-linac (ERL) machines. Any driving source of beam performance limitations in such a high-brightness electron beam transport system must be carefully examined in order to preserve the beam phase-space quality. Among those, we have already known the longitudinal space charge force (LSC) and coherent synchrotron

radiation (CSR) can particularly drive MBI. The LSC effect stems from upstream ripples on top of the longitudinal charge density and can accumulate an amount of energy modulation when the beam traverses a long section of a beam line. When the beam encounters bending, CSR due to electron coherent radiation emission inside a bend can have a significant effect on further amplifying the induced density modulations. A typical transport line in a recirculation machine can have a long linac or straight section and a large number of bending dipoles and thus can potentially incubate such density-energy conversion along the beam line. The successive accumulation and conversion mechanism between density and energy modulations can result in serious microbunching amplification, or MBI.

Numerical treatments of MBI can be divided into two categories: time-domain and frequency-domain methods. One of the time-domain treatments, or the most common one, is based on particle tracking. Particle tracking simulation (see, for example, [1,2]) with inclusion of relevant collective effects can be valuable for beam dynamics studies. It allows general beam line lattice, yet requires careful treatment of various numerical parameters to ensure numerical convergence before the reliable results are obtained [3,4]. Another dedicated time-domain treatment is based on the Monte-Carlo particle method, as implemented in Ref. [5]. The time-domain treatment turns out to be considerably challenging when MBI becomes severe. To compare with the linear theory at the onset of MBI, the initially imposed density modulation needs to be small enough to remain in the linear regime while such

*jcytsai@vt.edu

Published by the American Physical Society under the terms of the Creative Commons Attribution 3.0 License. Further distribution of this work must maintain attribution to the author(s) and the published article's title, journal citation, and DOI.

modulation requires to be large enough to rise above the numerical noises originated from the limited number of simulation particles. This implies that a large number of simulation particles and long computation time are required for reaching convergent results of microbunching gain, and strenuous efforts are needed to do parametric studies for machine design or optimization in order to minimize microbunching effects. A direct solution of the (nonlinear) Vlasov equation for the 2D longitudinal phase-space distribution, based on the semi-Lagrangian approach, was studied by Venturini *et al.* [6]. The issue of numerical noise is resolved with this approach, but the transverse effects of beam intrinsic spread are only approximately counted. The formulation extended to full 4D or 6D becomes further intricate [5] and application to machine design would become prohibitively expensive. To accurately and efficiently quantify the direct consequence of MBI at the onset, characterized by the microbunching amplification factor or the microbunching gain, we have recently developed a semianalytical linear Vlasov solver [7] based on the frequency-domain treatment. This semianalytical approach transforms the linearized Vlasov equation to an integral equation and solves for the bunching factor, and allows the proper inclusion of the transverse effects of beam intrinsic spread. The involvement of transverse beam emittances, causing Landau damping, was confirmed [8–10] to be an effective stabilizing mechanism for MBI. Our work extended the existing theoretical formulation [9,10] and included more relevant collective effects, including LSC, CSR and linac geometric effects, using analytical impedance expressions [11–26]. Since we do not directly solve the phase-space distribution function using mesh, the numerical noise issue is not a limiting factor and the numerical computation is much faster than the aforementioned treatments. This allows us to perform parametric design studies and machine optimization. The limitations of our Vlasov solver are the assumptions that (1) the microbunching modulation amplitude is much smaller than the unperturbed bunch density amplitude, i.e., in the linear growth regime of Vlasov equation or at the onset of MBI, and (2) beam line optics is linear.

For the rest of this paper, we introduce theoretical formulation of microbunching gain analysis in Sec. II. Then we briefly summarize in Sec. III the impedance models used in our Vlasov simulations. In Sec. IV, we describe numerical procedures for solving the Volterra-type integral equation for the bunching factor evolution. For illustration, we apply our code in Sec. V to two isochronous arcs and one combined lattice with an arc followed by a long section of linac, which are typical constituents for a recirculation machine. There we show the gain functions and gain spectra for the beam lines and their dependences on lattice optics, with combinations of various collective effects. We also discuss the underlying physics in the same section and finally summarize our observation from the simulation results in Sec. VI.

II. SEMIANALYTICAL FORMULATION FOR MICROBUNCHING ANALYSIS

We begin in this section by highlighting the existing theory and introducing our new development. Microbunching theory in a single-pass system was early developed by Saldin *et al.* [8], Heifets *et al.* [9], and Huang and Kim [10]. Saldin *et al.* [8] treated this problem as a klystron-like instability, considered the case without bunch compression, and assumed high-gain approximation. Then, Heifets *et al.* [9] extended the treatment including bunch compression as well as finite transverse beam emittance. Applying the standard perturbation technique to linearize the Vlasov equation and the method of characteristics, Heifets *et al.* derived a linear integral equation in terms of the bunching factor. Almost at the same time, Huang and Kim [10], by an iterative approach, obtained an analytical formula that can be used to estimate the CSR microbunching gain for a typical magnetic bunch compressor chicane. The above work was largely based on the linearized Vlasov equation and assumed constant energy along the beam line. Among them, we believe the integral equation derived in Refs. [9,10] can be further extended and applied to a general transport line.

In our work, to systematically study the microbunching gain development in a recirculating machine, we have extended the theoretical formulation [9,10] and incorporated more relevant physical models by: (i) including both transverse horizontal and vertical bending, in which the horizontal bends for recirculation arcs and vertical bends for spreaders and recombiners; (ii) allowing beam acceleration or deceleration for energy boosting or recovery; (iii) adding more relevant collective effects in addition to the steady-state free-space CSR that was considered in Refs. [8–10]. Here we distinguish in three viewpoints our work in this paper from the existing work done in the early days. First, although there have been extensive studies on microbunching dynamics, e.g., phase space fragmentation (see, for example, [27] and references therein), they mostly focus on bunch compressors in a linac-based free-electron laser (FEL) driver. There are still very limited works reported on quantitative microbunching gain studies in transport arcs or recirculation machines. To our knowledge, Borland first [28] did some preliminary studies of microbunching gains on the Advanced Photon Source (APS) upgrade ERL machine using ELEGANT [1] tracking with several collective effects included. Further understanding of the underlying physics would require a more detailed study of the contribution of each individual physical mechanism as well as careful benchmarking of particle tracking results with theory. Thus, more focused studies of the longitudinal microbunching gain with numerical benchmarking also serve as a purpose of our work. Second, the intuitive argument of quantifying microbunching in a beam line as the product of partial gains in each concatenated section is in general not self-consistent and the gain is found to be

underestimated [29]. Our Vlasov solver, incorporated with ELEGANT [1], adopts a general linear beam line lattice and all relevant beam and lattice parameters to treat the microbunching analysis in a consistent way. This also allows us to systematically study the impact of lattice optics on MBI. Third, by virtue of the general purpose of ELEGANT [1], our Vlasov solver can serve as an option for machine optimization if MBI would be a concern in the beam line design.

In the following we present the general theoretical formulation of the Vlasov analysis of microbunching instability, extended from the work by Huang and Kim [10]. To quantify MBI in a general linear transport line, we estimate the microbunching amplification factor $G(s)$ along the beam line. Here $G(s)$ is defined by the modular ratio of bunching factors g_k at a location s to the initial location $s = 0$ [see Eqs. (11) and (20) below]. The bunching factor $g_k(s)$ at a certain location s is defined as the Fourier transform of the perturbed phase-space distribution, a complex quantity in general. Based on the kinetic-model description and the standard linearization technique, the (linearized) Vlasov equation can be formulated and rewritten in an integral form in terms of bunching factors [9,10]. To facilitate simulating ERL-based lattices, which usually contain vertical spreaders and recombiners, we have extended the existing formulation to include both transverse horizontal and vertical bending. Furthermore, the presence of any linac section in a beam line is considered.

We begin by defining the six-dimensional phase-space coordinate as $\hat{X} = (\hat{x}, \hat{x}', \hat{y}, \hat{y}', \hat{z}, \hat{\delta})$, in which the prime denotes the derivative with respect to s and $\hat{\delta} = [E - E_r(s)]/E_0$. Of our interest, we consider a general case that beam energy can vary along a beam line. The formulation is reduced to that obtained in Refs. [9,10] for constant beam energy. The corresponding Hamiltonian for pure optics lattice transport can be expressed as

$$H_0 = \frac{1}{2} \left(K_x \hat{x}^2 + \hat{x}'^2 + K_y \hat{y}^2 + \hat{y}'^2 + \kappa \hat{z}^2 - 2\sqrt{\frac{E_0}{E_r}} \frac{\hat{x} \hat{\delta}}{\rho_x} - 2\sqrt{\frac{E_0}{E_r}} \frac{\hat{y} \hat{\delta}}{\rho_y} \right), \quad (1)$$

where K_x and K_y are horizontal and vertical focusing functions, respectively. $E_r(s)$ is the reference energy at s , and $E_0 = E_r(s = 0)$ is the initial energy. $\rho_x(s)$ and $\rho_y(s)$ are the bending radii of the horizontal and vertical dipoles. $\kappa = \frac{\Delta E_{\text{cav}} \omega_{\text{rf}}}{E_0 L_{\text{cav}} c} \cos \phi_s$ with ΔE_{cav} , ϕ_s , ω_{rf} and L_{cav} , respectively, the energy gain, synchronous phase, the angular frequency and the length of the accelerating cavity.

The corresponding single-particle equations of motion are [6]

$$\begin{aligned} \frac{d\hat{x}}{ds} &= \hat{x}', & \frac{d\hat{x}'}{ds} &= -K_x(s)\hat{x} + \sqrt{\frac{E_0}{E_r(s)}} \frac{\hat{\delta}}{\rho_x(s)} \\ \frac{d\hat{y}}{ds} &= \hat{y}', & \frac{d\hat{y}'}{ds} &= -K_y(s)\hat{y} + \sqrt{\frac{E_0}{E_r(s)}} \frac{\hat{\delta}}{\rho_y(s)} \\ \frac{d\hat{z}}{ds} &= -\sqrt{\frac{E_0}{E_r(s)}} \left(\frac{\hat{x}}{\rho_x(s)} + \frac{\hat{y}}{\rho_y(s)} \right), & \frac{d\hat{\delta}}{ds} &= -\kappa(s)\hat{z}. \end{aligned} \quad (2)$$

We note that the above equations of motion assume the rate of energy gain or loss is slow, i.e., adiabatic acceleration (or, deceleration), $E_r^{-1} dE_r/ds \ll 1$.

The general solution to Eq. (2) can be expressed in terms of a six-by-six transport matrix as

$$\hat{X}(s) = \hat{R}(s' \rightarrow s) \hat{X}(s') = \hat{R}(s) \hat{X}(0), \quad (3)$$

where $\hat{R}(0 \rightarrow s) \equiv \hat{R}(s)$. Here only linear elements are taken into account; effects of nonlinear elements such as sextupoles are excluded from the current analysis.

As mentioned in this section, all the information regarding the beam parameters and lattice configuration are adopted from ELEGANT [1], in which the 6D phase-space coordinate can be referred to be $X = (x, x', y, y', z, \delta)$, with the relation to our notation as

$$\begin{aligned} \begin{bmatrix} \hat{x} \\ \hat{y} \end{bmatrix} &= \begin{bmatrix} x \\ y \end{bmatrix} \sqrt{\frac{E_r(s)}{E_0}}, \\ \begin{bmatrix} \hat{x}' \\ \hat{y}' \end{bmatrix} &\simeq \begin{bmatrix} x' \\ y' \end{bmatrix} \sqrt{\frac{E_r(s)}{E_0}}, \\ \hat{z} &= z; & \hat{\delta} &= \delta + 1 - \frac{E_r(s)}{E_0}, \end{aligned} \quad (4)$$

where the prime denotes the derivative with respect to s and $\delta \equiv (E - E_0)/E_0$. We note that at $s = 0$, $\hat{X}(0) = X(0)$. When the beam energy is constant, $\hat{X}(s) = X(s)$ for all s . The relation between the conventional transfer matrix elements R_{ij} and \hat{R}_{ij} here can be obtained from Eq. (4) with $\hat{R}_{ij} = \sqrt{\frac{E_r}{E_0}} R_{ij} \delta_{ij}$ where $i, j = 1, 2, 3, 4$ and $\hat{R}_{ij} = R_{ij} \delta_{ij}$ for $i, j = 5, 6$, δ_{ij} is the Kronecker delta function.

The governing equation for the phase-space distribution function f is formulated by the Vlasov equation,

$$\frac{df}{ds} = \frac{\partial f}{\partial s} + \{f, H_0 + H_1\} = 0, \quad (5)$$

where $\{, \}$ denotes Poisson bracket and H_1 accounts for collective effect. The phase-space distribution function is normalized according to

$$\int f(X; s) dX = \int f(\hat{X}; s) d\hat{X} = N. \quad (6)$$

Here N is the total number of particles in the bunch. The solution to the equation can be an arbitrary function of the system Hamiltonian. Here we apply the standard perturbation technique by assuming $f = f_0 + f_1$, where $f_1 \ll f_0$. We further assume the initial unperturbed phase-space distribution is of the form

$$f_0(\hat{X}_0) = \frac{n_0}{(2\pi)^2 \varepsilon_{x0} \varepsilon_{y0} \sqrt{2\pi} \sigma_{\delta 0}} \times e^{-\frac{\hat{x}_0^2 + (\beta_{x0} \hat{x}'_0 + \alpha_{x0} \hat{x}_0)^2}{2\varepsilon_{x0} \beta_{x0}} - \frac{\hat{y}_0^2 + (\beta_{y0} \hat{y}'_0 + \alpha_{y0} \hat{y}_0)^2}{2\varepsilon_{y0} \beta_{y0}} - \frac{(\delta_0 - h \hat{z}_0)^2}{2\sigma_{\delta 0}^2}}, \quad (7)$$

where $n_0 = N/L$, with L the total bunch duration, ε_{x0} and ε_{y0} are the horizontal and vertical geometric emittances, respectively, α_{x0} , α_{y0} , β_{x0} and β_{y0} the initial Twiss or Courant-Snyder parameters, $\sigma_{\delta 0}$ for the rms uncorrelated (or, slice) relative energy spread assuming Gaussian energy distribution, and h for the chirp parameter (assuming $\hat{z} > 0$ for the bunch head).

In the absence of collective effect, i.e., only pure optics, from Eq. (5), the phase-space distribution function at s can be determined by the initial distribution at $s = 0$ [10],

$$f(\hat{X}; s) = f[\hat{R}^{-1}(s)\hat{X}(s); 0] = f_0(\hat{X}_0). \quad (8)$$

Assume there exists small density modulation in the initial beam phase-space distribution, i.e.,

$$f(\hat{X}_0) = f_0 + f_1 = \left(1 + \frac{\Delta n(\hat{z}_0)}{n_0}\right) f_0(\hat{X}_0). \quad (9)$$

We now would like to consider the collective effect due to this initial modulation. For small density-modulation-induced perturbation occurring within an infinitesimal time interval $d\tau$, the perturbed distribution function can be Taylor expanded to first order (or, the linearized Vlasov equation). The integrated effect over the entire particle trajectory is then [10]

$$f(\hat{X}; s) = f_0(\hat{X}_0) - \int_0^s d\tau \frac{\partial f_0(\hat{X}_\tau)}{\partial \hat{\delta}_\tau} \frac{d\hat{\delta}}{d\tau}, \quad (10)$$

where $\frac{d\hat{\delta}}{d\tau} = \frac{-Nr_e}{\gamma_\tau} \int \frac{dk_1}{2\pi} Z(k_1; \tau) g_{k_1}(\tau) e^{ik_1 \hat{z}_\tau}$ with r_e the classical radius of electron, γ the relativistic factor, Z the impedance per unit length, and g_k the so-called bunching factor defined as

$$g_k(s) \equiv \frac{1}{N} \int f(\hat{X}; s) e^{-ik_z \hat{z}_s} d\hat{X}. \quad (11)$$

Substituting Eq. (10) into Eq. (11), integrating over \hat{X}_τ by parts, and tracing variables back to initial [by applying Eq. (8)] gives the following integral equation:

$$g_k(s) = g_k^{(0)}(s) + \frac{ik_z(s)r_e}{\gamma_0} \int d\tau \hat{R}_{56}(\tau \rightarrow s) \int \frac{dk_1}{2\pi} Z(k_1; \tau) g_{k_1}(\tau) \int d\hat{X}_0 f_0(\hat{X}_0) e^{-ik_z \hat{z}_s(X_0) + ik_1 \hat{z}_\tau(X_0)}. \quad (12)$$

The integrations over k_1 and \hat{X}_0 can be analytically done; then Eq. (12) can be expressed in a compact form as the Volterra-type integral equation,

$$g_k(s) = g_k^{(0)}(s) + \int_0^s d\tau K(\tau, s) g_k(\tau), \quad (13)$$

where

$$g_k^{(0)}(s) = g_k^{(0)}(0) e^{-\frac{k^2(s)\varepsilon_{x0}\beta_{x0}}{2} [\hat{R}_{51}(s) - \frac{\alpha_{x0}}{\beta_{x0}} \hat{R}_{52}(s)]^2 - \frac{k^2(s)\varepsilon_{x0}}{2\beta_{x0}} \hat{R}_{52}^2(s) - \frac{k^2(s)\varepsilon_{y0}\beta_{y0}}{2} [\hat{R}_{53}(s) - \frac{\alpha_{y0}}{\beta_{y0}} \hat{R}_{54}(s)]^2 - \frac{k^2(s)\varepsilon_{y0}}{2\beta_{y0}} \hat{R}_{54}^2(s) - \frac{k^2(s)\sigma_{\delta}^2}{2} \hat{R}_{56}^2(s)} \quad (14)$$

and

$$K(\tau, s) = \frac{ik_0 I_0 C(s)}{\gamma_0 I_A} C(\tau) \hat{R}_{56}(\tau \rightarrow s) Z[k_0 C(\tau), \tau] \times [\text{Landau damping}], \quad (15)$$

where the expression of [Landau damping] term is

$$\exp \left\{ \frac{-k_0^2}{2} \left[\begin{aligned} &\varepsilon_{x0}\beta_{x0}(\hat{R}_{51}(s, \tau) - \frac{\alpha_{x0}}{\beta_{x0}}\hat{R}_{52}(s, \tau))^2 + \frac{\varepsilon_{x0}}{\beta_{x0}}\hat{R}_{52}^2(s, \tau) + \\ &\varepsilon_{y0}\beta_{y0}(\hat{R}_{53}(s, \tau) - \frac{\alpha_{y0}}{\beta_{y0}}\hat{R}_{54}(s, \tau))^2 + \frac{\varepsilon_{y0}}{\beta_{y0}}\hat{R}_{54}^2(s, \tau) + \sigma_\delta^2\hat{R}_{56}^2(s, \tau) \end{aligned} \right] \right\} \quad (16)$$

with

$$\hat{R}_{56}(\tau \rightarrow s) = \hat{R}_{55}(\tau)\hat{R}_{56}(s) - \hat{R}_{55}(s)\hat{R}_{56}(\tau) + \hat{R}_{51}(\tau)\hat{R}_{52}(s) - \hat{R}_{51}(s)\hat{R}_{52}(\tau) + \hat{R}_{53}(\tau)\hat{R}_{54}(s) - \hat{R}_{53}(s)\hat{R}_{54}(\tau) \quad (17)$$

$$\hat{R}_{5i}(s, \tau) = C(s)\hat{R}_{5i}(s) - C(\tau)\hat{R}_{5i}(\tau) \quad (18)$$

and the bunch compression factor $C(s)$ at s is defined as

$$C(s) = \frac{1}{\hat{R}_{55}(s) - h\hat{R}_{56}(s)}. \quad (19)$$

Other parameters shown in the above equations are: $k_0 = k_z(s=0)$ is the initial wave number ($=2\pi/\lambda$), I_0 for initial (peak) beam current, and I_A for Alfvén current. Here relevant collective effects $Z[k_0 C(\tau), \tau]$ are included in the kernel function $K(\tau, s)$, $g_k(s)$ is the resultant bunching factor as a function of the longitudinal position s , given a wave number k , and $g_k^{(0)}(s)$ is the bunching factor in the absence of collective effect, i.e., a factor due to the pure optics effect. We note that the above formulation can be applicable to the case with focusing in combined-function dipoles.

In the above formulation, we have made the coasting-beam approximation: the ripple wavelength on top of bunch charge density is assumed much shorter than the entire bunch duration. The transport functions $\hat{R}_{5i}(s)$ ($i = 1, 2, 3, 4, 5, 6$) can be obtained (e.g., from ELEGANT [1] in our code) by tracking a sufficient number of independent macroparticles and retrieving the six-by-six transport matrices at separate locations through proper transformations from the dynamic variables [see Eqs. (3) and (4)]. We notice that the validity of adiabatic acceleration (or deceleration, $E_r^{-1}dE_r/ds \ll 1$) in general may not be held when a beam is rapidly accelerated at very low energy.

Of our particular interest is the microbunching gain, as a function of the longitudinal coordinate s and the initial modulation wavelength λ (or, the initial wave number $k = 2\pi/\lambda$), and is defined as

$$G(s, k = 2\pi/\lambda) \equiv \left| \frac{g_k(s)}{g_k^{(0)}(0)} \right|. \quad (20)$$

Hereafter, we call $G(s)$, which is a function of s for a given modulation wave number, the *gain function* and refer to $G_f(\lambda)$ as the *gain spectrum*, a function of modulation wavelength at the exit location of a lattice (the subscript “ f ” indicates the exit of a beam line). It is worth mentioning the general physical meaning of Eqs. (13)–(16): a density perturbation at τ induces an energy modulation through the impedance $Z[k_0(\tau), \tau]$ and is subsequently converted into density modulation at s through the momentum compaction function $\hat{R}_{56}(\tau \rightarrow s)$. A brief introduction of numerical procedures to solve Eq. (13) would be highlighted later in Sec. IV.

III. IMPEDANCE MODELS

In this section we summarize relevant collective effects considered in our Vlasov solver, which includes CSR, LSC and linac geometric effects. For an electron beam traversing a finite-length dipole, CSR can have both steady-state and transient effects. In addition, when a beam goes through a long transport line, LSC can have a significant effect on accumulating energy modulations. Moreover, when a beam is accelerated, a long section of linac consisting of rf cavities is characteristic of the high-frequency geometric impedance, which can also accrue a certain amount of energy modulations. Here we quote the relevant impedance expressions without derivation.

A. CSR in free space and in parallel plate

For a relativistic electron beam ($\beta \rightarrow 1$, but $\gamma < \infty$) traversing a bending dipole, the free-space steady-state CSR impedance per unit length can be expressed as [11]

$$\begin{aligned} \text{Re}\{Z_{\text{CSR}}^{s,s,NUR}[k(s); s]\} &= \frac{-2\pi k(s)^{1/3}}{|\rho(s)|^{2/3}} \text{Ai}'\left(\frac{[k(s)|\rho(s)|]^{2/3}}{\gamma^2}\right) + \frac{k(s)\pi}{\gamma^2} \left(\int_0^{(k(s)|\rho(s)|)^{2/3}/\gamma^2} \text{Ai}(\varsigma) d\varsigma - \frac{1}{3} \right) \\ \text{Im}\{Z_{\text{CSR}}^{s,s,NUR}[k(s); s]\} &\simeq \frac{2\pi k(s)^{1/3}}{|\rho(s)|^{2/3}} \left\{ \frac{1}{3} \text{Bi}'(x) + \int_0^x \left[\text{Ai}'(x)\text{Bi}(t) \right] dt \right\}, \end{aligned} \quad (21)$$

where $x = [k(s)|\rho(s)]^{2/3}/\gamma^2$, $k = 2\pi/\lambda$ is the modulation wave number, $\rho(s)$ is the bending radius, and Ai and Bi are Airy functions. Under ultrarelativistic approximation ($\gamma \rightarrow \infty$), Eq. (21) is reduced to the well-known expression [12,13]:

$$Z_{\text{CSR}}^{s.s.UR}[k(s); s] = \frac{-ik(s)^{1/3}A}{|\rho(s)|^{2/3}},$$

$$A = -2\pi[Bi'(0)/3 + iAi'(0)]. \quad (22)$$

Prior to reaching the steady state, the beam entering a bend from a straight section would experience the so-called entrance transient state, where the impedance per unit length can be obtained by Laplace transformation of the corresponding wakefield [14,15]:

$$Z_{\text{CSR}}^{\text{ent}}[k(s); s] = \frac{-4}{s^*} e^{-4i\mu(s)} + \frac{4}{3s^*} [i\mu(s)]^{1/3} \Gamma\left(\frac{-1}{3}, i\mu(s)\right), \quad (23)$$

where $\mu(s) = k(s)z_L(s)$, s^* is the longitudinal coordinate measured from the dipole entrance, $z_L = (s^*)^3/24\rho(s)^2$, and Γ is the upper incomplete Gamma function.

There are also CSR exit transient effects when a beam exits from a dipole. For the case with CSR fields generated from an upstream electron (at retarded time, traveling along the upstream straight section) propagating across the dipole to downstream straight section, the corresponding impedance per unit length can be similarly obtained as Eq. (23) by Laplace transformation of the corresponding wakefield [16]:

$$Z_{\text{CSR}}^{\text{exit}}[k(s); s] = \frac{-4}{L_b + 2s^*} e^{\frac{-ik(s)L_b^2}{6|\rho(s)|^2}(L_b + 3s^*)}, \quad (24)$$

where s^* is the longitudinal coordinate measured from dipole exit and L_b is the dipole length. Other quantities are defined the same as above.

For the impedance expression of the case where CSR fields generated from an electron (at retarded time) within a dipole propagating downstream the straight section, we adopt the following expression for the CSR exit transient impedance [17]:

$$Z_{\text{CSR}}^{\text{drif}}[k(s); s] \approx \begin{cases} \frac{2}{s^*}, & \text{if } \rho^{2/3}\lambda^{1/3} \leq s^* \leq \lambda\gamma^2/2\pi \\ \frac{2k(s)}{\gamma^2}, & \text{if } s^* \geq \lambda\gamma^2/2\pi \\ 0, & \text{if } s^* < \rho^{2/3}\lambda^{1/3}, \end{cases} \quad (25)$$

where s^* is again the longitudinal coordinate measured from the exit of the dipole. This expression assumes the CSR fields come primarily from coherent edge radiation in the near-field region (i.e., $s^* < \lambda\gamma^2$). Moreover, in our

simulation we only include the exit transient effects at a nearby upstream bend.

Here we note that the above CSR impedance models are valid only when the wall shielding effect is negligible. This shielding effect becomes important when the distance from the beam orbit to the walls $h/2$ satisfies $h \leq (\rho\lambda^2)^{1/3}$. In this situation, one should consider to use the shielded CSR impedance in evaluating the CSR-induced micro-bunching gains. Currently we implement the steady-state CSR impedance based on the parallel-plate model [18,19], given by

$$Z_{\text{CSR}}^{\text{p.p.}}(k) = \frac{8\pi^2}{h} \left(\frac{2}{k(s)\rho(s)}\right)^{\frac{1}{3}} \sum_{p=0}^{\infty} F_0(\beta_p), \quad (26)$$

where $\beta_p = (2p+1)\frac{\pi}{h}\left(\frac{\rho(s)}{2k^2(s)}\right)^{\frac{1}{3}}$ and $F_0(\beta) = Ai'(\beta^2) \times [Ai'(\beta^2) - iBi'(\beta^2)] + \beta^2 Ai'(\beta^2)[Ai(\beta^2) - iBi(\beta^2)]$ and h is the full height of the vertical displacement of beam pipe.

In the above impedance expressions, the impedance depends on the beam line coordinate and the wave number k . Also the wave number depends again on the beam line coordinate, e.g., if bunch compression is involved, and the impedance is evaluated for a fixed wavenumber. The impedances [Eqs. (21)–(26)] assume a beam with a constant wave number and a bend with constant radius at each location s .

B. LSC in free space

Below we present two slightly different LSC impedance expressions implemented in our Vlasov solver. The first one is the *on-axis* model, which assumes a transversely uniform density with circular cross section of radius r_b [20],

$$Z_{\text{LSC}}^{\text{on-axis}}[k(s); s] = \frac{4i}{\gamma r_b(s)} \frac{1 - \xi K_1(\xi)}{\xi}, \quad (27)$$

where $\xi = \frac{k(s)r_b(s)}{\gamma}$ and $r_b(s) \approx \frac{1.747}{2} [\sigma_x(s) + \sigma_y(s)]$ [21]. The second one is the *average* model, which integrates the radial dependence of the space charge field [22],

$$Z_{\text{LSC}}^{\text{ave}}[k(s); s] = \frac{4i}{\gamma r_b(s)} \frac{1 - 2I_1(\xi)K_1(\xi)}{\xi}. \quad (28)$$

In the following we will use the on-axis model, in accordance with the built-in LSC impedance expression in ELEGANT [23].

In Eqs. (27) and (28), the longitudinal field does neither take into account the offset of bunch centroid nor the transverse dependence of the field along the bunch. We note that the expressions are approximate and do not reflect the most general case.

TABLE I. Initial beam and Twiss parameters for Example 1 and Example 2 arc lattices.

Name	Example 1 (large R_{56} , global isochronous)	Example 2 (small R_{56} , local isochronous)	Unit
Beam energy	1.3	1.3	GeV
Bunch current	65.5	65.5	A
Normalized emittance	0.3	0.3	μm
Initial beta function	35.81	65.0	m
Initial alpha function	0	0	
Energy spread (uncorrelated)	1.23×10^{-5}	1.23×10^{-5}	

V. EXAMPLES

To illustrate the application of our microbunching gain analyses, in this section we consider three different lattice examples, two high-energy recirculation arcs [30] and one linac-arc combination. Tables I and II summarize initial beam parameters used in our simulations. The first two lattice examples are isochronous arcs with the identical lattice geometry (here termed Example 1 and Example 2 lattices). In the last example, the linac-arc combination, the linac section is followed by Example 1 arc. In this third example, the electron beam is accelerated from 50 MeV to 1.11 GeV through a long section of linac which includes 200 accelerating cavities with the voltage gradient 10 MV/m, rf frequency 1497 MHz and on-crest acceleration. The purpose in this section is to demonstrate the microbunching gain evolution along a general beam line with inclusion of relevant collective effects and beam acceleration and to elucidate the underlying physics behind the simulation results.

A. Recirculation arcs

The first two 1.3 GeV high-energy recirculation arcs are considered as comparative examples. Figure 1 shows the optical lattice functions and the momentum compaction functions across the arcs. Although both lattices have the same geometric layout, they exhibit distinct magnetic optical behaviors upon adjusting sets of quadrupole focusing strengths. Here the Example 1 lattice is a 180° arc with large momentum compaction \hat{R}_{56} . Moreover, it is a

TABLE II. Initial beam parameters for the linac-arc example lattice.

Name	Value	Unit
Beam energy (at linac entrance)	50	MeV
Beam energy (at linac exit)	1.11	GeV
Peak bunch current	88	A
Normalized emittance	0.3	μm
Initial beta function	18	m
Initial alpha function	-3.6	
Energy spread (uncorrelated)	$\sim 3 \times 10^{-4}$	

second-order achromat and globally isochronous with a large dispersion modulation across the entire arc [see Figs. 1(a) and 1(c)]. By contrast, the Example 2 lattice is again a 180° arc with however small momentum compaction. This arc is also a second-order achromat but is designed to be a locally isochronous lattice within superperiods. Such local isochronicity ensures that the bunch length be kept the same at phase homologous CSR emission sites [see Figs. 1(b) and 1(d)]. Notably, it is shown in Figs. 1(c) and 1(d) that the momentum compaction function $\hat{R}_{56}(s)$ for the Example 2 lattice is considerably smaller in amplitude compared with that for Example 1 because of local isochronicity. For the detailed description of the design for the two example lattices, we refer the interested reader to Ref. [30].

For both examples, the (peak) beam current is chosen to be 65.5 A, the transverse normalized emittances are assumed 0.3 μm , and the uncorrelated energy spread is set 1.23×10^{-5} . Other relevant initial Twiss beam parameters are shown in Table I. In these two examples, we simply *turn on* CSR effects [Eqs. (21)–(26)] and in particular studied the CSR-induced microbunching gains for the two arcs. Figures 2 and 3 show the CSR-induced microbunching gain functions and gain spectra, respectively, for the two arcs. The two upper figures present the gain functions $G(s)$ as a function of s for two different modulation wavelengths with a different combination of CSR models. One can see in Fig. 2 the shorter wavelengths enhance Landau damping through Eq. (16), while longer wavelengths feature a negligible CSR effect. The two bottom figures show the gain spectra $G_f(\lambda)$ at the exits of the lattices as a function of initial modulation wavelength. A major difference between the two examples is observed that Example 1 is vulnerable to the CSR microbunching whereas the microbunching gain in Example 2 remains around unity (i.e., there is no microbunching amplification). To validate our linear Vlasov results, we benchmark the two example lattices by using ELEGANT [1,3], with which extensive convergence studies were performed [4]. Both our semianalytical solutions and ELEGANT tracking results show good agreement in microbunching gain estimation (see Figs. 2 and 3).

From the bottom part of Fig. 2, we find that the microbunching gain including both steady-state and

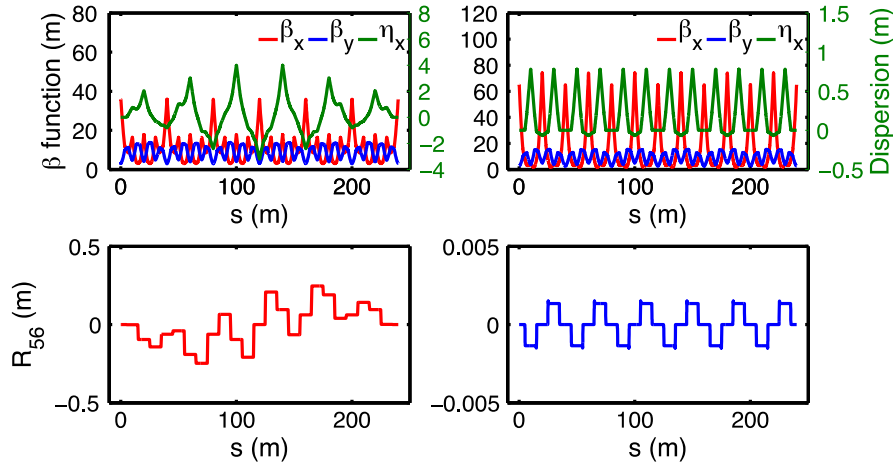


FIG. 1. Twiss and R_{56} transport functions for 1.3 GeV high-energy transport arc: (a) and (c) with large momentum compaction function R_{56} (Example 1); (b) and (d) with small momentum compaction function R_{56} (Example 2). Note in the two cases $\hat{R}_{56} = R_{56}$.

entrance transient CSR effects is slightly lowered from the case of steady-state CSR alone. This is because the CSR impedances including entrance transient effect become a bit reduced near the dipole entrance when the beam traverses

across the bend. We also observe that with the inclusion of all relevant CSR effects, the microbunching gain increases about 400% compared with that of the steady-state case. This indicates that without optical compensation the CSR exit transient effect can make a significant contribution on

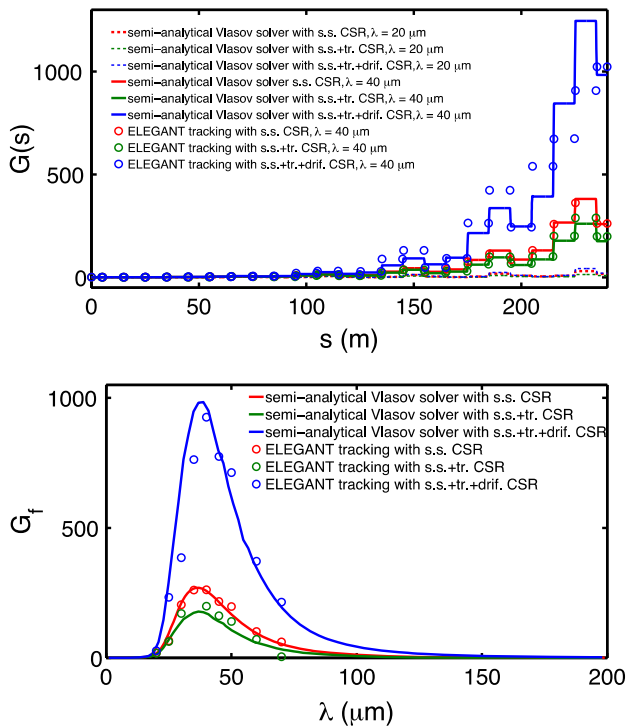


FIG. 2. (Top) Gain functions $G(s)$ as a function of s , where the dashed lines are for $\lambda = 20 \mu\text{m}$ and solid lines for $\lambda = 40 \mu\text{m}$. (Bottom) Gain spectra $G_f(\lambda)$ as a function of initial modulation wavelength. In ELEGANT simulations (dots), the initial density modulation is set 0.05% for the steady-state case; 0.06% for the steady-state and the entrance-transient cases; 0.01%–0.04% for all relevant CSR effects including entrance, exit transients and steady-state CSR. With larger gain, to keep the microbunching process remaining in the linear regime, it is required the initial modulation amplitude be smaller (see also comments in the context).

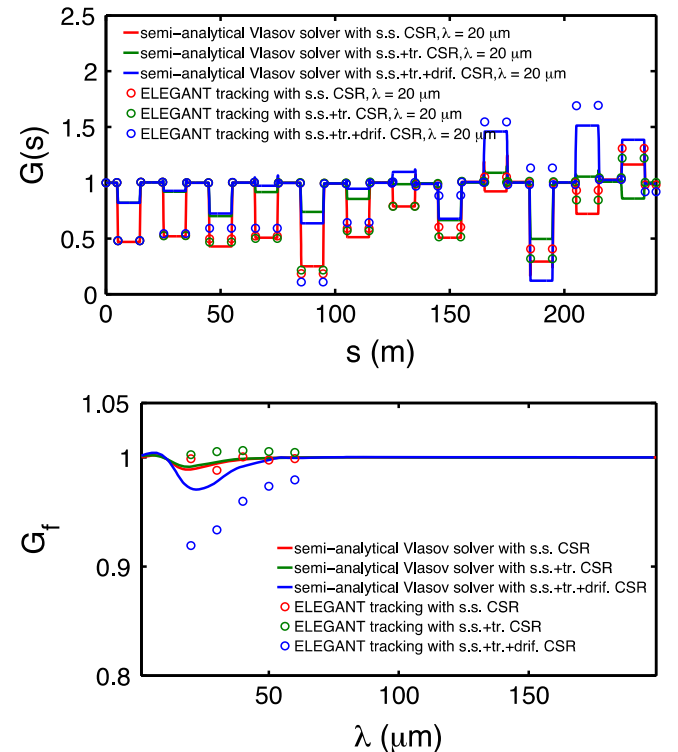


FIG. 3. (Top) CSR gain functions $G(s)$; (bottom) gain spectra $G_f(\lambda)$ as a function of initial modulation wavelength. Initial density modulations are all set 0.8% in ELEGANT tracking simulations. The apparent difference between Vlasov solutions and ELEGANT tracking is actually small; note the vertical scale in small numerics.

microbunching gain development. Yet with optical compensation, even with the same dipole configuration over the beam line, Example 2 is not subject to CSR-induced MBI (see Fig. 3). This highlights the impact of optical lattice design for recirculation arcs on microbunching gain development. Here we note that, because of extremely high gain of the Example 1 lattice when we include all relevant CSR impedances, ELEGANT tracking results were averaged over a range of initial modulation amplitudes 0.01%–0.04% and 70-million macroparticles were used in the tracking simulation. In postprocessing of ELEGANT tracking results, we determine the modulation amplitude at a specific location by the following procedures [32]: (i) make a z (or t) histogram from 6D phase space distribution while removing the leading and trailing part to eliminate possible edge effects; (ii) fit a polynomial to the remaining data and remove the constant offset; (iii) take Fourier transform of the fitted data and select the nominal modulation wavelength which is supposed to be dominant over a spectral range. The corresponding spectral amplitude is recorded as the relative modulation amplitude at that location. The microbunching gain is then calculated as the ratio of the current amplitude to the initial one (at $s = 0$). In Figs. 2 and 3 one can see good agreement of the microbunching gains from Vlasov solver and ELEGANT tracking. The reader is referred to Refs. [4,31,32] for more detailed and systematic convergence tests and postprocessing procedures to extract the microbunching gains from particle tracking data. We notice that with the large gain shown in Fig. 2 the microbunching mechanism may reach the non-linear regime where linearized Vlasov solutions are no longer valid from a practical point of view. For the validity of linear microbunching gain analysis using particle tracking, it is required that the initial perturbation be sufficiently small (although in some practical cases it may not be so small) that the magnitude of the bunching factor along the beam line should not exceed a certain value. Here we suggest a merit to our semianalytical Vlasov approach: since the microbunching gain obtained from particle tracking depends sensitively on the numerical parameters used for tracking (e.g., macroparticle numbers, meshes, bins, and etc.), benchmarking the semianalytical gain results with the tracking results could also help us to establish the suitable numerical parameters for particle tracking that would give convergent physical results.

B. Linac-arc combination

As the third example, we take a recirculation arc of Example 1, preceded by a long section of linac. Table II summarizes relevant beam parameters for the linac-arc combination lattice. Figure 4 shows the dispersion function and momentum compaction function along the entire beam line. It can be seen in Fig. 4 that the momentum compaction function has taken into account the nonultrarelativistic effect.

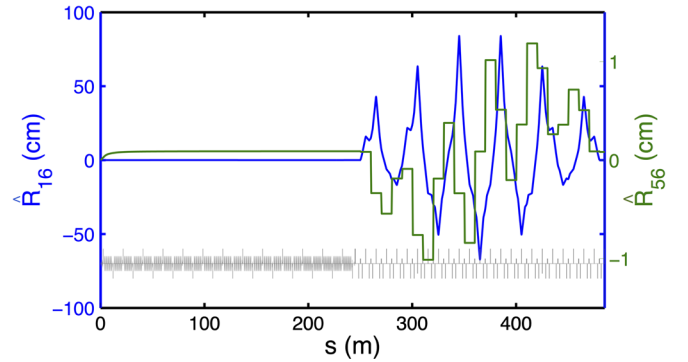


FIG. 4. Dispersion (blue) and momentum compaction (green) functions of the example linac-arc lattice.

Figures 5 and 6 show the evolution of microbunching gain functions $G(s)$ along the beam line. ELEGANT tracking simulations were performed for a Gaussian beam (over transverse phase-space and energy coordinates) of 70-million macroparticles and flat-top z -distribution with small density modulations on top. For consistency of comparison between our semianalytical solutions with ELEGANT results, the LSC effect is only applied within drift elements and rf cavities. The LSC effect within other elements such as dipoles and quadrupoles is neglected. In Fig. 6, CSR effects include both entrance transient and steady states inside individual dipoles, as well as exit transient effects in the downstream drift sections. We found in Fig. 5 the microbunching gain is slightly reduced in the linac section because of LSC-induced plasma oscillation along with beam acceleration. Our linear Vlasov solutions match well with ELEGANT tracking results throughout the lattice except at some *particular* locations (e.g., at $s = 410$ – 440 m, in Figs. 5 and 6). After carefully examining numerical parameters to ensure the convergence of ELEGANT tracking results, we found the microbunching gain deviation between our linear Vlasov solutions and ELEGANT results is not from numerical issues but originates from nonuniformity of the bunch profile as a result of

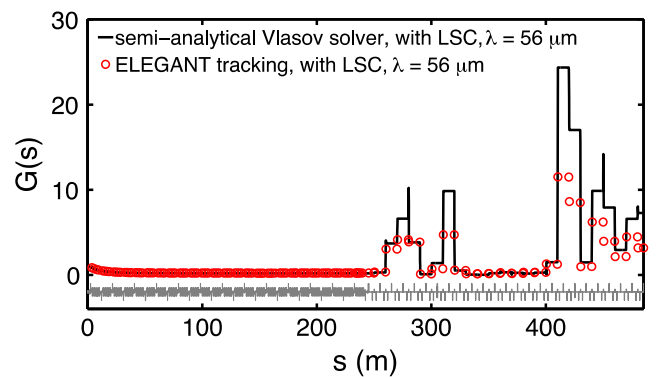


FIG. 5. LSC-induced microbunching gain function $G(s)$ for the linac-arc lattice. Here in ELEGANT tracking we assume 0.1% initial modulation amplitude.

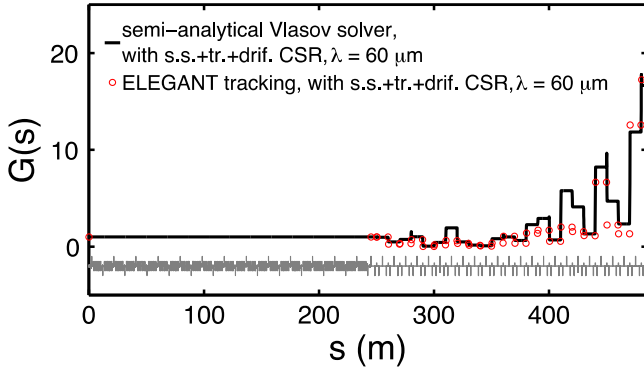


FIG. 6. CSR-induced microbunching gain function $G(s)$ for the linac-arc lattice. Here the CSR models include both entrance and exit transients as well as steady-state effects. Here in ELEGANT tracking we assume 0.6% initial modulation amplitude.

existing (nonlinear) rf curvature (see Fig. 7 for the longitudinal phase space distribution and projected longitudinal bunch profile). Here we assume this rf curvature from the linac is not compensated by a harmonic cavity, as usually used in linac-based FELs.

Here we would show that this bunch nonuniformity profile indeed causes the microbunching gain slightly reduced. The tracking results would be compared with our linear Vlasov solutions, which do exclude this effect from microbunching gain estimation. Because of the presence of an rf cavity, the accelerated beam is characteristic of a nonlinear rf curvature (see the top part of Fig. 7). In the case of on-crest acceleration, we can simply assume the particle energy deviation for each slice related to its longitudinal coordinate given by

$$\delta_i = hz_i + qz_i^2, \quad (33)$$

where the linear chirp h vanishes but the quadratic chirp q does exist (e.g., negative in our case). With such $(z - \delta)$ correlation, we can define an effective (local) chirp to be

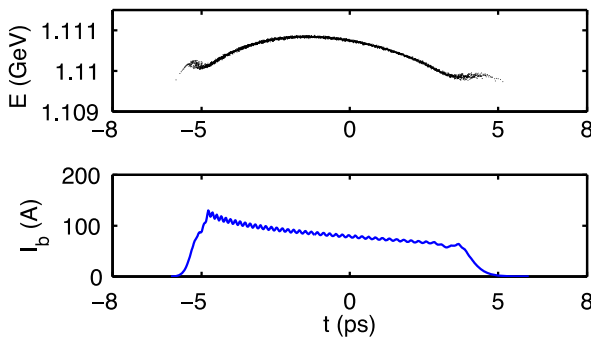


FIG. 7. (Top) Longitudinal phase space distribution at $s = 410$ m. (Bottom) Bunch current density. Note here the bunch head is to the left.

$$h^{\text{eff}}(z_i) \equiv -\frac{\partial \delta_i}{\partial z_i} = -2qz_i \Rightarrow \begin{cases} < 0, & \text{for bunch tail } (z_i < 0) \\ > 0, & \text{for bunch head } (z_i > 0). \end{cases} \quad (34)$$

For the head of the bunch, the effective chirp is positive whereas it is negative for the tail of the bunch. The local bunch compression factor can be described as

$$C(s, z_i) = \frac{1}{\hat{R}_{55}(s) - h^{\text{eff}}(z_i)\hat{R}_{56}(s)} \Rightarrow \begin{cases} > 1, & \text{for bunch head and } \hat{R}_{56}(s) > 0 \\ < 1, & \text{for bunch tail and } \hat{R}_{56}(s) > 0. \end{cases} \quad (35)$$

Note that, in the positive momentum compaction region, the modulation wavelength in the head portion of the bunch is lengthened (or, decompressed) while that in the tail of the bunch is shortened (or, compressed) due to the nonzero quadratic chirp, and vice versa in the negative momentum compaction region. It is this situation that results in the nonuniformity of the bunch profile when a beam is imprinted with a nonlinear chirp.

By the above simple analysis we can explain the presence of nonuniformity of bunch profile, as shown in Fig. 7. Note that in the figure the bunch head is to the left. The nonuniform density-modulated bunch profile broadens the spectral width around the nominal modulation frequency, and results in a reduced bunching factor as well as the corresponding microbunching gain.

Figures 8–10 show the microbunching gain spectra for cases with different collective effects involved. From Fig. 8, we can see the dependence of modulation wavelength on LSC-induced microbunching gain. In Fig. 9, both our Vlasov solver and ELEGANT include all relevant CSR effects, including both transient and steady states. We believe the deviation between the two methods comes from: (i) nonuniformity of the bunch profile; (ii) different

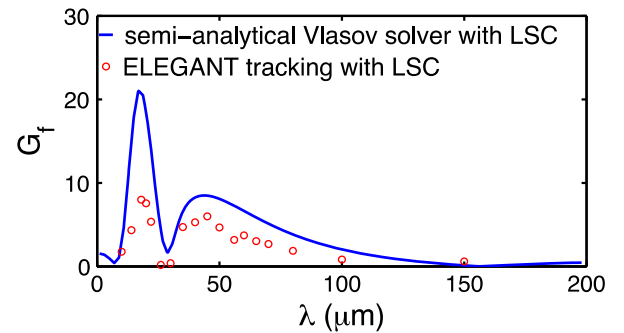


FIG. 8. Microbunching gain spectra with LSC effects. Note here that in ELEGANT simulation we vary the initial modulation amplitudes around 0.1%–0.6%.

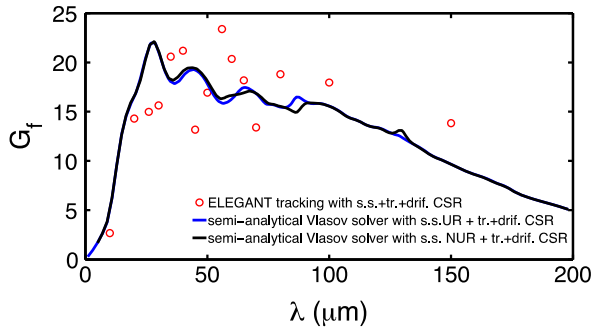


FIG. 9. Microbunching gain spectra with all relevant CSR effects. ELEGANT results include both entrance and exit transient as well as steady-state impedances. The initial modulation amplitudes are varied around 0.1%–0.6% to ensure numerical convergence.

models of CSR exit transient models used in our simulation [see Eqs. (24) and (25)] and in ELEGANT [1,16]. We also notice that the gain reduction of the nonultrarelativistic CSR (NUR, black curve) with the ultrarelativistic CSR (UR, blue curve) is negligible because CSR occurs at the high energy level. The fluctuations shown in Fig. 9 are from the CSR exit transient effects, which can be observed both in our linear Vlasov solutions and ELEGANT results. Here we notice that the exit transient CSR impedance model applied in our solver [Eq. (25)] still requires further improvement.

In Fig. 10 we consider altogether the collective effects for the microbunching gain calculation. We observe that the overall microbunching gain is in fact an accumulation effect of density-energy conversion throughout the beam line. In the long section of the upstream linac, LSC and linac geometric effects have accumulated an amount of energy modulation, and subsequently such energy modulation converts to density modulation through the

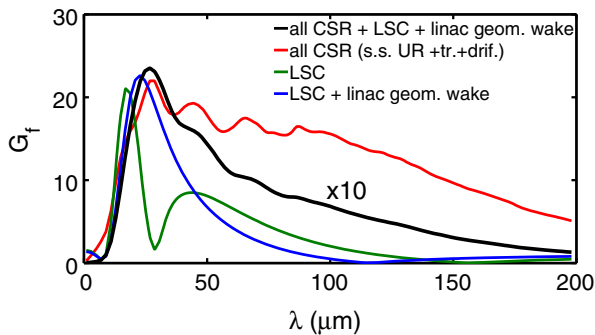


FIG. 10. Microbunching gain spectra with various combinations of collective effects. To simulate the gain with linac geometric impedance, here we assume the linac parameters are $a = 3.07$ cm, $L = 10.0$ cm, $g = 8.0$ cm, and $\alpha = 0.528$. For better illustration, the gain values with the case of all collective effects included (black curve) are presented with $\times 10$ smaller than the calculated values.

downstream momentum compaction. Then, the converted density modulation can be further amplified through the CSR effects downstream the arc.

To end this section, we would like to emphasize one advantage of using the newly developed Vlasov solver over particle tracking simulation (e.g., ELEGANT). To the authors' knowledge, it is not trivial in time-domain particle tracking to include all relevant collective effects such as CSR, LSC and the associated geometric effects into thorough consideration for MBI analysis. However, with our Vlasov solver, it is straightforward to add these relevant impedance models into consideration. Although we do not expect the Vlasov solver, based on evaluating collective impedance expressions, to give as rich information as ELEGANT tracking results do in microbunching analyses, we point out that the value of this solver lies in its speed in execution. This advantage makes the solver a powerful tool for comparative or parametric studies and for design optimization.

VI. SUMMARY

In this paper we have introduced the theoretical formulation for MBI analysis, which includes the case with beam energy change based on the scaled dynamical variables. The coasting-beam approximation was considered and the collective effects were treated as a perturbation in the theory. Then we summarized various collective impedance models relevant to the microbunching instability for our subsequent analysis. We also outlined the implemented numerical procedures to solve the governing equation for bunching-factor evolution. After that, we took three examples, two recirculation arcs and a linac-arc beam line, to demonstrate our microbunching gain calculation. From the simulation results, we conclude that different lattice optics can give dramatically different microbunching gains, albeit the geometric layout is identical. From the linac-arc example, our linear Vlasov solutions match well with ELEGANT tracking results except at the locations with large local momentum compaction. We identify that such local bunch compression comes from the nonuniformity of the bunch profile which stems from rf curvature existing in the upstream rf cavities, and can result in microbunching gain reduction. With inclusion of all relevant collective effects (i.e., CSR, LSC and linac geometric effects) in the linac-arc example, the results show that the overall microbunching gain can be significantly enhanced due to the energy-density conversion throughout the beam line.

While our newly developed linear Vlasov solver can be much more efficient [33] and accurate in calculating microbunching gain than using particle tracking, we would like to emphasize the limitations of the formalism upon which our solver bases. First, only the effects of linear beam line elements can be accounted for. For an ERL or specialized beam line design with sextupole or higher-order magnetic elements, their effects are overlooked in our

consideration. Second, for the case of large gain, e.g., Fig. 2, the linear Vlasov solver cannot be applied to the nonlinear regime or saturation. Third, since the formulation (and thus our Vlasov solver) is based on an integral equation governing the bunching factor g_k , it cannot provide as much information as particle tracking does, e.g., the detailed evolution of phase space distribution. Fourth, in the presence of beam acceleration (or deceleration), the method [6] we adopted assumes the rate of energy gain (or loss) is slow. This may not be valid for rapid acceleration at very low beam energy. Fifth, the LSC impedance model adopted in the solver is idealized and does neither account for bunch centroid offset nor transverse dependence along bunch slides. Further studies are under way in order to improve the formulation and impedance models for more general applications.

ACKNOWLEDGMENTS

This work is supported by Jefferson Science Associates, LLC under U.S. DOE Contract No. DE-AC05-06OR23177.

-
- [1] M. Borland, ELEGANT: A flexible SDDS-compliant code for accelerator simulation, APS Light Source Note LS-287 (2000).
 - [2] J. Qiang, R. Ryne, S. Habib, and V. Decyk, An object-oriented parallel particle-in-cell code for beam dynamics simulation in linear accelerators, *J. Comput. Phys.* **163**, 434 (2000).
 - [3] M. Borland, Controlling noise and choosing binning parameters for reliable CSR and LSC simulation in ELEGANT, Report No. OAG-TN-2005-027.
 - [4] C.-Y. Tsai and R. Li, Simulation of coherent synchrotron radiation induced microbunching gain using ELEGANT, Report No. JLAB-TN-14-016.
 - [5] G. Bassi, J. Ellison, K. Heinemann, and R. Warnock, Microbunching instability in a chicane: two-dimensional mean field treatment, *Phys. Rev. ST Accel. Beams* **12**, 080704 (2009).
 - [6] M. Venturini, Microbunching instability in a single-pass system using a direct two-dimensional Vlasov solver, *Phys. Rev. ST Accel. Beams* **10**, 104401 (2007).
 - [7] C.-Y. Tsai, D. Douglas, R. Li, and C. Tennant, Linear Vlasov solver for microbunching gain estimation with inclusion of CSR, LSC and linac geometric impedances, [arXiv:1508.04667](https://arxiv.org/abs/1508.04667).
 - [8] E. L. Saldin, E. A. Schneidmiller, and M. V. Yurkov, Klystron instability of a relativistic electron beam in a bunch compressor, *Nucl. Instrum. Methods Phys. Res., Sect. A* **490**, 1 (2002).
 - [9] S. Heifets, G. Stupakov, and S. Krinsky, Coherent synchrotron radiation instability in a bunch compressor, *Phys. Rev. ST Accel. Beams* **5**, 064401 (2002).
 - [10] Z. Huang and K.-J. Kim, Formulas for coherent synchrotron radiation microbunching in a bunch compressor chicane, *Phys. Rev. ST Accel. Beams* **5**, 074401 (2002).
 - [11] R. Li and C.-Y. Tsai, CSR impedance for nonultrarelativistic beams, *Proceedings of the 6th International Particle Accelerator Conference* (2015).
 - [12] J. B. Murphy, S. Krinsky, and R. L. Gluckstern, Longitudinal wakefield for an electron moving on a circular orbit, *Part. Accel.* **57**, 9 (1997).
 - [13] Ya. S. Derbenev, J. Rossbach, E. L. Saldin, and V. D. Shiltsev, Microbunch radiative tailhead interaction, TESLA-FEL Report No. 1995-05.
 - [14] D. Zhou, An alternative 1D model for CSR with chamber shielding, in *Proceedings of the 3rd International Particle Accelerator Conference, New Orleans, Louisiana, USA, 2012* (IEEE, Piscataway, NJ, 2012), MO0BB03.
 - [15] C. Mitchell and J. Qiang, Effects of transient CSR wakefields on microbunching in a bunch compressor, *Proceedings of the 4th International Particle Accelerator Conference* (2013).
 - [16] E. L. Saldin, E. A. Schneidmiller, and M. V. Yurkov, On the coherent radiation of an electron bunch moving in an arc of a circle, *Nucl. Instrum. Methods Phys. Res., Sect. A* **398**, 373 (1997).
 - [17] R. A. Bosch, Longitudinal wake of a bunch of suddenly accelerated electrons within the radiation formation zone, *Phys. Rev. ST Accel. Beams* **10**, 050701 (2007).
 - [18] R. Warnock, Shielded coherent synchrotron radiation and its effects on very short bunches, Report No. SLAC-PUB-5375, 1990.
 - [19] T. Agoh and K. Yoneda, Calculation of coherent synchrotron radiation using mesh, *Phys. Rev. ST Accel. Beams* **7**, 054403 (2004).
 - [20] M. Venturini, Models for longitudinal space charge impedance for microbunching instability, *Phys. Rev. ST Accel. Beams* **11**, 034401 (2008).
 - [21] J. Wu, Z. Huang, and P. Emma, Analytical analysis of longitudinal space charge effects for a bunched beam with radial dependence, *Phys. Rev. ST Accel. Beams* **11**, 040701 (2008).
 - [22] M. Venturini, M. Migliorati, C. Ronsivalle, M. Ferrario, and C. Vaccarezza, Dynamics of longitudinal phase-space modulation in an rf compressor for electron beams, *Phys. Rev. ST Accel. Beams* **13**, 080703 (2010).
 - [23] Z. Huang, M. Borland, P. Emma, J. Wu, C. Limborg, G. Stupakov, and J. Welch, Suppression of microbunching instability in the linac coherent light source, *Phys. Rev. ST Accel. Beams* **7**, 074401 (2004).
 - [24] R. L. Gluckstern, Longitudinal impedance of a periodic structure at high frequency, *Phys. Rev. D* **39**, 2780 (1989).
 - [25] K. Yokoya and K. Bane, The longitudinal high-frequency impedance of a periodic accelerating structure, in *Proceedings of the 18th Particle Accelerator Conference, New York, 1999* (IEEE, New York, 1999).
 - [26] Z. Huang, P. Emma, M. Borland, and K.-J. Kim, Effect of linac wakefield on CSR microbunching in the Linac Coherent Light Source, in *Proceedings of the 2003 Particle Accelerator Conference, Portland, OR* (IEEE, New York, 2003).
 - [27] Z. Huang, J. Wu, and T. Shaftan, Microbunching instability due to bunch compression, *ICFA Beam Dynamics Newsletters* **38**, 57 (2005).

- [28] M. Borland, Growth of density modulation in an energy recovery linac light source due to coherent synchrotron radiation and longitudinal space charge, *Proceedings of the 24th Linear Accelerator Conference* (2008).
- [29] C.-Y. Tsai and R. Li, Combination of density and energy modulation in microbunching analysis, *Proceedings of the 7th International Particle Accelerator Conference* (2016).
- [30] D. Douglas, S. V. Benson, A. Hutton, G. A. Krafft, R. Li, G. R. Neil, Y. Roblin, C. D. Tennant, and C.-Y. Tsai, Control of coherent synchrotron radiation, and microbunching effects during transport of high brightness electron beams, [arXiv:1403.2318v1](https://arxiv.org/abs/1403.2318v1); D. Douglas, S. V. Benson, A. Hoffer, R. Kazimi, R. Li, Y. Roblin, C. D. Tennant, G. A. Krafft, B. Terzic, and C.-Y. Tsai, Control of synchrotron radiation effects during recirculation, *Proceedings of the 6th International Particle Accelerator Conference* (2015).
- [31] C.-Y. Tsai and R. Li, Step-by-step guide to using `volterra_mat` and some notes on the code, Report No. JLAB-TN-15-019.
- [32] M. Borland, Modeling the microbunching instability, *Phys. Rev. ST Accel. Beams* **11**, 030701 (2008).
- [33] For example, each run in the bottom part of Fig. 2 (representing a dot from ELEGANT tracking) can take about 8 hours using a 16-node cluster computer. The same run only takes 20 seconds using our Vlasov solver in a laptop computer.